NASA Technical Memorandum 82753

Application of Surface Analysis to Solve Problems of Wear

Donald H. Buckley
Lewis Research Center
Cleveland, Ohio

Prepared for the
Ideelle Träger der SURTEC Berlin '81
Berlin, West Germany, June 29–July 3, 1981

NASA

APPLICATION OF SURFACE ANALYSIS TO SOLVE PROBLEMS OF WEAR

Donald H. Buckley
National Aeronautics and Space Administration
Lewis Research Center
Cleveland, Ohio, U.S.A.

ABSTRACT

In recent years many surface analytical tools have become available for use by the tribologist. Some of these devices can be used to follow structural and chemical changes that take place on surfaces during the wear process and thereby provide insight into wear mechanisms. Results are presented in this paper for the use of such surface tools including field ion microscopy, (FIM) Auger emission spectroscopy analysis (AES), cylindrical mirror Auger analysis (CMA) and X-ray photoelectron spectroscopy (XPS). Data from the field ion microscope reveal adhesive transfer (wear) at the atomic level with the formation of surface compounds not found in the bulk, and AES reveals that this transfer will occur even in the presence of surface oxides. Both AES and XPS reveal that in abrasive wear with silicon carbide and diamond contacting the transition metals the surface and the abrasive undergo a chemical or structural change which effects wear. With silicon carbide, silicon volitilizes leaving behind a pseudo-graphitic surface and the surface of diamond is observed to graphitize.

E-1069

INTRODUCTION

When two solid surfaces are brought into contact and relative motion occurs between those surfaces due to sliding, rolling or rubbing wear of one or both surfaces can result. If a load or force is applied to the solids normal to the interface between the solids wear will nearly always occur. The

quantity of material transferred or transported across the interface from one solid to another or removed as loose debris will depend upon on how effectively the solid surfaces are shielded from atomically intimate solid state contact by surface oxides, adsorbed species or lubricating films.

A host of surface analytical tools have been developed in recent years for the elemental, compound, structural and atomic definition of surfaces. One can do everything from identifying the structural position of single atoms on a solid surface with such devices as the field ion microscope and analyze the chemistry of that single atom with the atom probe to depth profiling the chemistry of surface layers of solids identifying all elements and compounds with such devices as XPS (X-ray photoelectron spectrosopy) with an ion gun.

Many of the currently available surface analytical tools have been used by the author and members of his research group in the study of wear. These tools have included the field ion microscope, atom probe, LEED (low energy electron diffraction), AES (Auger emission spectroscopy), cylindrical mirror Auger analysis (CMA), XPS (X-ray photoelectron spectroscopy), SEM (scanning electron microscopy) and energy dispersive X-ray analysis.

The objective of the present paper is to review the use of various surface analytical devices in identifying wear mechanisms and the progressive loss of material from surfaces in solid state contact. Many of the surface tools are incorporated directly into wear systems for an in situ analysis. Results are presented for both lubricated and unlubricated surfaces. Both changes in material properties at the surface and loss are examined. In addition the influence of surface films in wear is perceived with the aid of surface analysis.

APPARATUS

An apparatus used for in situ surface analysis is a vacuum system with the capability of the measurement of adhesion forces, friction, and also performing Auger, and LEED surface analysis. A diagram of such an apparatus is shown schematically in Fig. 1.

A gimbal mounted beam projects into a vacuum system. The beam contains two flats machined normal to each other with strain gages mounted thereon. The pin specimens are mounted on the end of the beam. A load is applied by moving the beam toward the disk. The normal force is measured by a strain gage. Adhesive forces are measured by moving the beam in the direction opposite to which the load was applied (see Fig. 1).

Tangential motion of the pin along the disk surface is accomplished through the gimbal assembly. Friction force is measured by the strain gage normal to that used to measure applied normal force. Full scale deflection on a conventional strip chart recorder results from a 10 g load.

Multiple wear tracks could be generated on the disk surface by translating the beam containing the pin. Pin sliding was in the vertical direction in Fig. 1.

In addition to the friction apparatus the experimental chamber also had a LEED (low energy electron diffraction) system and an Auger spectrometer. The electron beam of both could be focused on any disk site.

The vacuum system was a conventional vacsorb and ion pumped system capable of readily achieving pressures of $10^{-8} N/m^2$ as measured by a nude ionization gage. Sublimation pumping was also used.

A second type of apparatus used for multiple repeated passes across the surface with continuous monitoring of changes in surface chemistry using cylindrical mirror Auger analysis is shown schematically in figure 2.

The friction and wear specimens consisted of a disk specimen 6.5 centimeters in diameter and 1.2 centimeters thick and a hemispherical rider with a 0.5-centimeter radius. The specimens are shown in the apparatus schematic of figure 2. The disk specimen is mounted on a drive shaft which is rotated with a magnetic drive assembly. The drive assembly provides for rotation at various speeds. The rider specimen is mounted in an insulated holder to one end of a stainless-steel shaft. Friction and wear experiments are conducted with the rider specimen loaded against the disk surface. As the disk is rotated, the rider scribes a circular wear track on the flat surface of the disk. The loads used vary from 100 to 1000 grams.

Experiments are conducted in a vacuum (see fig. 2). The vacuum system is pumped by sorption pumps and an ion pump. Pressure in the vacuum system is read with a nude ionization gage. The vacuum system achieved a pressure of 1×10^{-8} N/m^2 after bakeout at 250° C.

The friction force between the disk and rider specimens is continuously recorded during the experiment. The beam which contains the rider specimen is welded into a bellow assembly which is gimbal mounted to the vacuum system. The gimbal mounting permits deadweight loading of the rider against the disk surface (fig. 2). At right angles to the deadweight loading, the beam containing the rider can move in two directions in the horizontal plane. Movement of the rider (with the disk as it rotates) is restrained by a cable which is attached to a beryllium-copper ring. The ring contains four sets of strain gages. These gages measure the frictional force between the disk and rider specimens. The friction force is recorded on a strip chart.

The disk specimens are finish ground on metallurgical papers to a grit of 600. They are then diamond polished with 6-micrometer and finally

3-micrometer diamond paste. The disks are rinsed with acetone and then with absolute ethyl alcohol.

The specimens are cleaned by ion bombardment in the experimental chamber. The disk specimen is insulated from ground on the drive shaft. Two copper rods are brought to the disk from feed-throughs insulated from ground. The end of one rod terminates 0.5 centimeter from the circumferential edge of the disk specimen. This terminal establishes the positive potential in the glow discharge. The second rod has a beryllium-copper leaf attached to it. The end of the leaf opposite its attachment to the rod makes a wiping type of contact with the circumferential edge of the disk. The entire flat of the disk is cleaned by the sputtering as a result of being immersed in the glow discharge. The specimens are ion-bombarded by bleeding research-grade argon gas into the system until a pressure of about 2 N/m^2 is achieved. A direct-current power supply is used to supply 400 to 500 volts between the disk and the floating electrode. With the negative potential on the disk positively charged, argon ions bombard and sputter clean the specimen surfaces. Variations in the argon pressure can alter the voltage necessary for efficient sputtering. The higher the pressure, the lower the voltage needed.

Elemental analysis of the disk specimen surface can be made before, during, and after the friction and wear experiment by using an Auger cylindrical mirror analyzer with an integral electron gun. The point of rider to disk contact passes under the Auger beam 20 seconds after the disk moves out of the contact zone. This time period can be reduced by increasing the speed at which the disk rotates. The disk could rotate over a broad range of speed, and Auger analysis could still be performed. The Auger analyzer is a commercial unit.

The primary beam of electrons is directed at the disk surface by a beam from the electron gun in the Auger cylindrical mirror analyzer. The beam is focused on the wear track scribed by the rider in sliding contact with the disk. The beam contact is 180° away from the rider on the disk surface. The beam spot diameter is 0.2 millimeter. The gun contains deflection plates which allow positioning of the beam on the disk surface.

The secondary electrons come off the specimen surface, pass through a cylindrical can opening, and then pass through slits in an inner cylinder which serves as an energy analyzer. They are collected by an electron multiplier. Elemental identification is accomplished by analysis of the detected secondary-electron energies. The Auger electrons that appear in the secondary-electron distribution "fingerprint" the surface elements to a depth of approximately four atomic layers.

Auger traces are displayed on an oscilloscope. The sweep control module permits a full-spectrum scan for those elements of interest in friction, wear, and lubrication in 0.10 second. Thus, there exists the capability of monitoring a moving or rotating surface and detecting dynamic variations in surface chemistry.

Figures 1 and 2 are representative figures of devices used for measuring friction and wear while providing a geometry amienable for in-situ surface analysis. Other configurations are used in the author's laboratory for surface analysis such as the conduction of adhesion experiments directly in the field ion microscope. In discussing data the appropriate references will be cited for those interested in more apparatus detail. All such devices are reviewed in reference 1.

RESULTS AND DISCUSSION

Adhesion at the Atomic Level

Conduction of adhesion experiments in the field ion microscope permit the observation of the adhesion and wear process at the atomic level.[2,3] Figure 3(a) is a field ion micrograph of a tungsten surface, asperity free, prior to contact with a gold flat. Each individual white spot of figure 3 represents an individual atom site on the solid surface and the rings represent atomic planes. Figure 3(b) is that same surface after having been contacted by gold. Gold adheres to the tungsten surface. If the imaging voltage for the surface is increased some of the gold field evaporates from the tungsten surface revealing clusters of gold atoms adhered to the tungsten as indicated in figure 3(c). In such clusters, there is adhesive bonding to the tungsten and cohesive bonding of the gold atoms to each other. Additional field evaporation removes all the gold and reveals the parent tungsten.

Gold and tungsten do not form compounds and gold is essentially insoluble in tungsten[4] and yet gold bonds to the surface of tungsten. The bonding of gold to tungsten can not be mechanical in nature because the tungsten is free of asperities. It can not be electrostatic in nature because the field ionization voltages should cause a loss of the gold below the 14.5 kV required for field evaporation in figure 3(c). It must, therefore, be concluded that the gold is chemically bonded. The chemistry and physics of metallic interfaces are not dependent on the conventions of bulk metal behavior.

Gold and rhodium do not form compounds.[5] Sliding friction experiments with the apparatus of figure 1 however, indicates that gold will adhere to rhodium. This is shown in the Auger emission spectrum obtained on the rhodium surface contacted by gold in figure 4. Auger peaks occur for both rhodium and gold, are present indicating gold transfer.

Simple adhesion experiments with gold contacting iridium in the field ion microscope revealed an ordered transfer of gold to the iridium surface. There is very limited solid solubility of gold in iridium and no compound formation.[5] Gold decorates ledge sites and with field evaporation is removed last from the (100) plane.[3]

The results obtained with gold contacting tungsten, rhodium and iridium indicate that bulk properties and bulk behavior may not apply directly to surface considerations. While there is limited or no solubility of gold in tungsten, rhodium, or iridium, gold adheres and transfers to the surface of these metals.

Transfer of gold to the surface of the tungsten, rhodium, and iridium in the surface clean state indicates that adhesion has occurred at the interface between the bimetallic couple and that the interfacial adhesive bond is stronger than the cohesive bonding in the cohesively weaker of the two metals, namely the gold. When the interfacial bonding and the adjacent surficial layers are pulled in tension fracture occurs in the gold with gold remaining adhered to the other surface. This constitutes a loss of material from the parent material and wear.

There are a number of factors which will contribute to quantity of metal which will transfer from one surface to another. First, there is the actual size of the discrete points of solid state contact which make up the real area of contact between the solids. The larger the cross sectional area of these contacts the greater the number of adhesive bonds.

Factors which shall influence the real contact area will include the applied load or force with which the surfaces are pressed into contact, the surface and bulk elastic properties of the metals, plastic behavior and to a

limited extent topography. These factors are important with respect to both metals of the bimetallic couple.

If two metal single crystal of the same material have the identical surface orientation, their surfaces are atomically clean and perfect matching of planes and direction could be achieved as the surfaces approached one another a single metal crystal free of any detectable interface would occur. As a practical matter such a condition is never achieved and the minimal interfacial defect will be a grain boundary for like materials is contact. Many of the concepts that apply to such boundaries, apply then to the interface.

The greater the degree of disregistry across the interface the greater will be the amount of lattice strain in the surficial layers of both solids and the greater will be the nature and number of interface defects including dislocations, vacancies, etc. Further, the greater the degree of interfacial mismatch the greater is the degree of boundary energy.[6]

When the interfacial region of the adhered solids is pulled in tension fracture will occur in the atomically structurally weakest zone. This generally is subsurface in one of the two solids. The depth and location will be determined by the extent of lattice strain and the location of subsurface defects. With inorganic solids in sliding friction experiments, fracture was observed in the zone of the subsurface maximum shear stress where there was an intersection of slip bands and dislocation coalescence.[7]

Where dissimilar solids make adhesive contact, one of the two solids may experience the greater amount of lattice strain, presence of defect structures, etc. Generally, this occurs in the cohesively weaker of the two materials which will undergo lattice strain to accommodate the applied force

and to come into lattice registry with the cohesively stronger material for chemical bonding.

The presence of the naturally occurring oxides on metal surfaces can inhibit strong adhesion. When, however, tangential motion is initiated, oxide layers can be penetrated and metal transport across the interface will occur. This is demonstrated in the Auger emission spectroscopy data on figure 5 where gold was observed to have transferred to a palladium surface containing an oxide. Both oxygen and gold peaks were observed in addition to palladium.

Gold does not form a stable oxide. With metals that do strong bonding of a clean metal to oxide surface can and will occur. Under such conditions the adhesive force is often a function of the force necessary to separate the metal from oxygen.[8]

The foregoing is a guide relative to the transport of metals in contact indicating in a fairly predictable manner, metal will transfer from one surface to another in adhesive contact. With relative tangential motion between the surfaces as with sliding, rolling, or rubbing interfacial transport becomes more complex. Under such conditions, plastic deformation, shear and high surface temperatures due to frictional heating are but some factors which must be given attention. At relatively modest conditions of sliding, for example, surface temperatures of from 50° to 1000° C are easily achieved on metal surfaces.[9] Such temperatures can modify or alter interfacial behavior.

Sliding Experiments with silicon carbide/iron system

Silicon carbide is a material of interest in abrasion and has been examined in sliding contact. Sliding friction experiments were conducted with single-crystal silicon carbide in contact with iron in vacuum. Friction-force traces resulting from such sliding were generally characterized by a

stick-slip behavior.[18] All the coefficients of friction presented in figure 6 are static values. The coefficient of static friction μ is defined: $\mu = F_1/W$, where F_1 is the friction force at which the first break, that is, first motion is observed in the friction-force trace and W is the normal load. The kinetic friction is defined: $\mu_k = F/W$, where F is the friction force determined by averaging the heights of maximum peaks in the friction-force trace, and W is the normal load. The kinetic friction properties of silicon carbide in sliding contact with iron were almost the same as those shown in figure 6.

The coefficient of friction of the silicon carbide {0001} surfaces in contact with iron as a function of sliding temperatures is indicated in figure 6. The iron rider was sputter cleaned with argon ions. The silicon carbide was in the as-received state after it had been baked out in the vacuum system. The specimen was then heated to the sliding temperature before the friction experiment was initiated. The coefficient of friction increased slightly with increasing temperature at temperatures below 400° C. Above 400° C, the coefficient of friction decreased with an increase in temperature in the range of 400° to 600° C. The general decrease in friction at these temperatures is due to the gradual removal of the contaminants of carbon and oxygen from the surface. The coefficient of friction increased with increasing temperature in the range of 600° to 800° C. The increase in friction at these temperatures can be associated with increased adhesion and increased plastic flow in the area of contact. Above 800° C the coefficient of friction decreases rapidly with an increase of temperature. The rapid decrease in friction above 800° C was analyzed using Auger emission spectroscopy and XPS (X-ray photoelectron spectroscopy).

An Auger electron spectrum of the silicon carbide surface obtained before heating is presented in figure 7. The surface was in the as-received state. A carbon peak due to contamination was evident as well as an oxygen peak.

Spectra of surfaces heated to 250°, 400°, and 600° C revealed that the silicon carbide surface contained impurities, such as sulfur, oxygen, nitrogen, etc. Auger peaks for carbon, however, indicated a carbide-type carbon peak. The spectrum of the surface heated to 800° C (fig. 8) is the same as that obtained for an argon sputter cleaned surface[11]. Contamination peaks have disappeared from the spectrum; and, in addition to the silicon peak, Auger peaks indicate a carbide-type carbon on the surface of silicon carbide.

The spectra of the surface heated to 1500° C (fig. 9) clearly reveal two characteristics: (1) a graphite-type carbon peak and (2) a decrease in the silicon peak with increasing temperature. The carbide-type carbon peak changed to a graphite type at 900° to 1000° C, while the silicon peak decreased in intensity. The decrease of silicon peak intensity is due to preferential evaporation of silicon from the silicon carbide. The mechanism for graphite formation is that two successive carbon layers on the surface of silicon carbide, after evaporation of silicon, collapse into one layer of carbon hexagons with the unit mesh parallel to that of silicon carbide (refs. 12 and 13).

Figures 7 to 9 also show the typical Auger carbide-type, graphite-type, and amorphous carbon peaks. The carbide-type peaks are characterized by three sharp peaks labelled A_0, A_1, and A_2 in figure 8, where A is used to denote an Auger peak. The graphite form is characterized by a step, where it's position is labelled A in figure 9. Amorphous carbon appears only as the single main carbon peak labelled A_0 shown in figure 7.

The XPS (X-ray photoelectron spectroscopy) spectra of the C_{1s} and Si_{2p} obtained from narrow scans on the single-crystal silicon carbide surface are presented in figures 10 and 11. All the XPS spectra were taken at room temperature after bake out and preheating. The Si_{2p} photoelectron peak energies associated with silicon carbide at the various temperatures undergo a gradual change from 16.06 aJ (100.4 eV) (at the bake out temperature of 250° C) to 16.0 aJ (100.0 eV) (at 1500° C preheating temperature). The vertical height, peak to base line, of the Si_{2p} peak in the spectra were minimum at the bake out temperatures and were the highest at 800° C. They were nearly the same at the temperatures of 400° and 600° C. But above 800° C the Si_{2p} for silicon carbide decreased gradually with increasing temperature.

The photoelectron emission lines for C_{1s} of the silicon carbide are split asymmetrically into doublet peaks (figs. 10 and 11). The results show a significant influence of temperature on the silicon carbide surface. Three spectral features, which are dependent on the chemical nature of the specimen, are observed: (2) two kinds of doublet peaks, (2) change of the vertical height of the peaks, and (3) shift of peaks.

The doublet peaks are due to distinguishable kinds of carbon, that is, (1) a carbon contamination peak and a carbide peak at the room temperature, and (2) the graphite and the carbide peaks at temperatures from 400° to 1500° C. The XPS spectra of the as-received specimens are shown in figure 10. The peak height of the carbon contamination is higher than that of carbide. At 250° C, the primary peaks are the adsorbed amorphous carbon contamination and carbide, and the contaminant peak height is lower than that of the carbide. For specimen preheated to 400° C the carbon contamination peak disappears from the spectrum. The graphite and carbide peaks are seen in the spectra of the specimens preheated to 400° C and above. Both the peak heights of graphite

and the carbide are increased with an increase of preheating temperatures. A large carbide peak is distinguished at a temperature of 800° C.

The AES analysis of silicon carbide surface preheated at a temperature of 800° C indicated that (1) the AES spectrum is the same as that obtained for an argon sputter cleaned surface and (2) the spectrum includes carbide-type carbon as well as a silicon peak on the surface. The spectrum indicates that the surface is pure silicon carbide. But XPS analysis, which can provide more detailed chemical information than AES, clearly indicates the presence of graphite on the silicon carbide surface preheated to 800° C.

At 900° C the carbide peak height was smaller than that at 800° C, but the graphite peak height was larger. The carbide peak height, however, was still larger than that of the graphite. At 1000° C the height of carbide peak decreased and became smaller than that of the graphite. further, at 1500° C the height of carbide peak becomes very small. A very large graphite peak, however, is observed.

The AES analysis of the silicon carbide surface preheated to 1500° C (fig. 9) indicated that the silicon AES peak had almost disappeared and that the carbon peak shown was only that of graphite. But XPS analysis (fig. 11) indicates evidence for silicon and carbide being present as well as graphite on the silicon carbide surface preheated to 1500° C. This difference can be accounted for by the fact that XPS analysis depth is deeper and is more sensitive to the presence of silicon than is AES.

The graphitization behavior in the outermost surficial layer of silicon carbide is believed to be as follows. The analysis depth with AES is of the order of 1 nm or less and an elemental concentration as low as 0.1 percent of a monolayer can be detected and identified. The analysis depth with XPS is of the order of 2 nm or less, and the ultimate sensitivity is sufficient to allow

fractions of a monolayer to be detected and identified. Therefore, the outermost surficial layer, which consists of mostly graphite and very little silicon, on the silicon carbide surface is concluded to be of the order of 1 nm.

Thus, the use of surface analytical tools (AES and XPS) to study the silicon carbide surface reveals that the cause for the reaction of friction at 800° C in figure 6 is the graphitization of the silicon carbide surface which occurs with heating. The AES and XPS analysis complimented each other in the determination. These experimental results (figures 6 through 11) reveal the value of surface analytical tools in the characterization of tribological surfaces.

Sliding Experiments with diamond/iron system

Another example of the usefulness of surface tools in the examination of surfaces in sliding contact is that for diamond in sliding contact with metals. Diamond, like silicon carbide can vary in it's surface composition and this variance will influence friction behavior. The diamond surface was Argon sputter cleaned and examined with Auger emission spectroscopy prior to friction studies.

The main features of the carbon peaks of the Auger spectra from diamond are shown in figure 12. An Auger electron spectroscopy spectrum of a single-crystal diamond 111 plane obtained before argon-ion bombardment is shown in figure 12(a).

The crystal was in the as-received state after it had been baked out in the vacuum system. A carbon contamination peak is evident, and the spectrum is similar to that of amorphous-carbon. The surface was next argon-ion bombarded at a 3-kilovolt potential, under a pressure of approximately 7×10^{-4} Pa for 15, 30, 45, and 60 minutes.

The spectrum of the surface after 15-minutes has three peaks, which are characteristic of graphite. The spectra of the surface after 30, 45 and 60 minutes have four peaks, which are characteristic of diamond. Thus, graphitizaion of a diamond surface can occur just as it does for silicon carbide.

The peaks have been labelled A_0 to A_3, as was done with silicon carbide in figure 8. The energy of the peaks in this experiment were 267 to 269 for A_0, 252 to 254 for A_1, 240 eV for A_2, and 230 to 232 eV for A_3. The spectra of figure 12(d) is that of a clean diamond surface[14].

Thus, for the adhesion and friction experiments, the surfaces of the diamond were argon-ion bombarded for 45 to 60 minutes under the pressure of approximately 7×10^{-4} Pa, and the Auger spectra of the surfaces were very similar to that shown in figure 12(d).

Once one knows the real nature of the clean solid surface, then meaningful tribological experiments can be conducted. With the diamond surface fundamental relationships have been sought between metallic properties and the friction behavior of those metals in contact with a clean diamond surface.

The data in figure 13 indicate the coefficients of friction for some of the transition metals in contact with a single-crystal diamond 111 surface as a function of the d-bond character of the metal. The percentage of d-bond character can be related to the chemical affinity of the surfaces. The greater the percentage of d-bond character that the metal possesses, the less active its surface should be. The data indicates a decrease in friction with an increase in d-bond character. When titanium and zirconium, which are chemically very active, are in contact with diamond, they exhibit very strong interfacial adhesive bonding to diamond. In contrast, rhodium and rhenium,

which have a very high percentage of d-bond character have relatively low coefficients of friction.

Figure 13 also presents the friction data for a diamond surface in sliding contact with a yttrium surface. Yttrium gives a higher coefficient of friction than that estimated from data of other metals. This may be due to the effect of oxygen. An argon-sputter-cleaned yttrium surface was covered by an oxide surface layer.

It is very difficult to remove the oxide surface layer from yttrium by argon-sputter cleaning. The effects of oxygen in increasing the friction is related to the relative chemical thermodynamic properties and bonding of carbon to oxygen. The greater the degree of bonding across the interface, the higher the coefficient of friction. In the case of yttrium, oxygen on the surface tends to strongly chemically bond the yttrium to the diamond surface.

Adhesion and friction properties of the transition metals sliding on other nonmetals, such as silicon carbide, boron nitride and manganese-zinc ferrite are the same as observed for the metals in sliding contact with diamond[14]. The more active the metal, the higher the coefficient of friction. There appears to be very good agreement between friction and chemical activity for the transition metals in vacuum.

Surface Films and Their Effect on Tribological Behavior

Sliding friction experiments were conducted in the apparatus shown schematically in figure 2 with elemental iron exposed to various extreme pressure type lubricating compounds for the purposes of in situ analysis with Auger emission spectroscopy.

It has been established that the antiwear properties of chlorine-containing additives depend very strongly on the labile nature of the carbon-to-chlorine bond. The antiwear properties improve with decreasing

strength of the carbon-to-chlorine bond (ref. 15). The chlorine atom in benzyl chloride is highly reactive since it is joined to the alkyl group rather than to the benzene ring. An alkyl-aryl compound is more reactive than the alkyl halide ethyl chloride (ref. 16). Thus, it is a good candidate for examination.

Since during the sliding or rubbing process associated with two metals in contact nascent metals are exposed, experiments were conducted with clean iron surfaces. The iron disk specimen was sputter-cleaned with argon ion bombardment. A typical Auger spectrum for a clean iron surface is presented in figure 14(a). There are four Auger energy peaks in the spectrum associated with iron, one low-energy and three high-energy peaks. There is a complete absence of other elements on the iron surface.

The surface of figure 14(a) was exposed to 10^{-2} torr-second (10^{4} langmuirs) of benzyl chloride. The resulting Auger spectrum is presented in figure 14(b). The same four iron peaks are present as in figure 14(a), and in addition there is a peak associated with the presence of chlorine on the surface. The chlorine comes from the benzyl chloride. Note in figure 14(b) that there is no indication of the presence of carbon on the surface. If carbon were present, an Auger peak would appear in the spectrum between the chlorine and the first of the three high-energy iron peaks.

Auger emission spectroscopy is particularly sensitive to the presence of carbon on surfaces. Very small amounts of carbon on an iron surface can be readily detected by Auger analysis (ref. 17). Thus, if carbon were present on the iron, it should have appeared in the spectrum of figure 14(b).

The absence of carbon on the iron surface indicates that benzyl chloride adsorbs dissociatively. The molecule dissociates with the chlorine remaining chemisorbed to the iron surface and the hydrocarbon portion of the molecule

going into the vacuum system. Benzyl choride needs only to contact a clean iron surface for iron chloride to form.

The amount of chlorine on the iron surface is a direct function of the exposure or concentration of benzyl chloride. This is evidenced by the data of figure 15. Results are presented in figure 15 for exposure to benzyl chloride, both static and during sliding. At each exposure a greater concentration of chlorine absorbs on the surface during sliding. Sliding contact thus promotes dissociative adsorption.

The coefficient of friction continuously decreases with increasing exposure to benzyl chloride. This is seen in the friction data of figure[16]. Thus, the more chlorine present on the iron surface, the lower the friction.

The data of figure 16 were obtained at a load of 100 grams. Chlorine when reacted with iron is purportedly a good extreme-pressure lubricant; that is, it is an effective boundary lubricant at heavy loads. In order to determine the tenacity of chloride films formed from benzyl chloride, experiments were conducted at various loads with a chloride film formed by exposure of iron to 10^{-2} torr-second (10^{4} langmuirs) of benzyl chloride. Sliding was conducted repeatedly over the same track. Changes in Auger chlorine peak intensity with repeated passes over the same surface at three loads are presented in figure 17.

An examination of figure 17 indicates that a 100-gram load sliding over the same surface to 100 repeated passes does not change very notably the chlorine surface coverage. With a load of 300 grams, however, the Auger chlorine peak intensity continuously decreases with successive passes over the surface. After 100 passes the chlorine peak intensity is approximately one-half the intensity prior to the commencement of sliding.

If the load was increased from 300 to 1000 grams in the sliding friction experiments, even further reductions in chlorine peak intensity were observed, as indicated in the data of figure 17. At only 27 passes the Auger chlorine peak intensity is less than one-third the value obtained before the start of sliding. After 100 passes, while chlorine is still present on the surface, a considerable amount has been removed during sliding.

It should be indicated that the Auger beam spot diameter is 0.6 millimeter, and at the light load of 100 grams the beam is sampling not only the wear track but also a region to either side of it. Notwithstanding this fact, chlorine is still being removed from the surface, as evidenced by the Auger data of figure 17. At the heavier loads of 300 and 1000 grams a wear track will develop more rapidly.

There are three possible explanations for the reductions in chlorine peak intensity with sliding shown in figure 17. Any one or all three may be contributing to the reduction observed in chlorine peak intensity. First, sufficient interfacial energy may develop at the interface to cause dissociation of the iron chloride into iron and chlorine. This mode of chlorine removal appears unlikely because of the stability of iron chloride.

Second, chlorine removal may involve the burial of the chloride film by metallic iron. As load is increased and with repeated passes, an increasing amount of iron-to-iron contact occurs through the film. Elemental iron being relatively soft, it flows plastically very readily. With an increasing exposure of the area scanned by the primary electron beam consisting of iron there is an accompanying decrease in the amount of chloride being sampled.

Third, the film may simply be reduced in thickness with repeated passes. The sliding process is simply wiping chloride out of the contact zone. This latter mechanism appears to be the most plausible.

Concluding Remarks

The use of surface analytical tools presently available to the tribologist provide insight into wear mechanisms and lubrication of surfaces. Some specific observations made include:

1. Adhesion studies in the field ion microscope reveal that atomic level adhesive transfer can occur with compound formation developed on the surface not seen in bulk alloying. The specific metals discussed herein were tungston in contact with gold. Similar results, have however been observed with other metal couples.

2. Adhesive metal transfer as observed with Auger emission spectroscopy analysis even occurs in the presence of surface oxides.

3. Both Auger emission spectroscopy analysis and X-ray photoelectron spectroscopy reveal in the study of abrasive wear with silicon carbide and diamond contacting metals that surface chemical changes take place to the abrasive which alters friction and wear behavior. Graphitization of these surfaces is observed.

4. The interaction of lubricants with solid surfaces can be continuously monitored with such surface tools as cylindrical mirror Auger analysis during wear studies. Results obtained with benzyl chloride indicate that the mechanical surface activity of sliding can promote surface reactions to occur. Variations in the surface loading can modify the concentration of the antiwear additive on the surface.

REFERENCES

1. Buckley, D. H.: Surface Effects in Adhesion Friction, Wear and Lubrication. Tribology Series, Vol. 5. Elsevier, 1981.

2. Miller, E. W.; and Tsong, T. T.: Field Ion Microscopy. American Elsevier Publishing Co. Inc., 1969.

3. Brainard, W. A.; and Buckley, D. H.: Preliminary Studies by Field Low Microscopy of Adhesion of Platinum and Gold to Tungsten and Ludrium. NASA TN D-6492, 1971.

4. Hansen, M.: Constitution of Binary Alloys. Second ed. McGraw-Hill Book Co. Inc., 1958.

5. Elliott, R. P.: Constitution of Binary Alloys. First Supplement, McGraw-Hill Book Co. Inc., 1965.

6. McLean, D.: Grain Boundaries in Metals. Clarendon Press, (Oxford), 1957.

7. Buckley, D. H.: Friction, Wear, and Lubrication in Vacuum. NASA SP-277, 1971.

8. Buckley, D. H.: Adhesion of Metals to a Clean Iron Surface Studied With LEED and Auger Emission Spectroscopy. Wear, vol. 20, 1972, pp. 89-103.

9. Bowden, F. P.; and Tabor, D.: The Friction and Lubrication of Solids. Part I. Oxford Univ. Press, 1950.

10. Miyoshi, K.; and Buckley, D. H.: Changes in Surface Chemistry of Silicon Carbide (0001) Surface With Temperature and Their Effect on Friction. NASA TP-1756, 1980.

11. Miyoshi, K.; and Buckley, D. H.: Effect of Oxygen and Nitrogen Interactions on Friction of Single-Crystal Silicon Carbide. NASA TP-1265, 1978.

12. Badami, D. V.: X-Ray Studies of Graphite Formed by Decomposing Silicon Carbide, Carbon, vol. 3, no. 1, 1965, pp. 53-57.

13. Van Bommel, A. J.; Crombeen, J. E.; and Van Tooren, A.: LEED and Auger Electron Observations of the SiC (0001) Surface. Surf. Sci., vol. 48, no. 2, 1975, pp. 463-472.

14. Miyoshi, K.; and Buckley, D. H.: Tribological Properties and Surface Chemistry of Silicon Carbide at Temperatures to 1500° C. Prepared for ASLE Trans. April 30, 1981.

15. Forbes, Eric S.: Antiwear and Extreme Pressure Additives for Lubricants. Tribology, vol. 3, no. 3, Aug. 1970, pp. 145-152.

16. Brewster, Ray Q.; and McEwen, W. E.: Organic Chemistry. Second ed. Prentice Hall, Inc., 1959.

17. Buckley, Donald H.: Friction-Induced Surface Activity of Some Hydrocarbons With Clean and Oxide-Covered Iron. NASA TN D-7233, 1973.

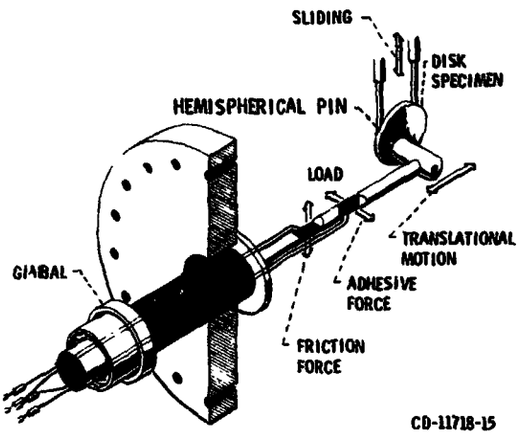

Figure 1. - High-vacuum friction apparatus.

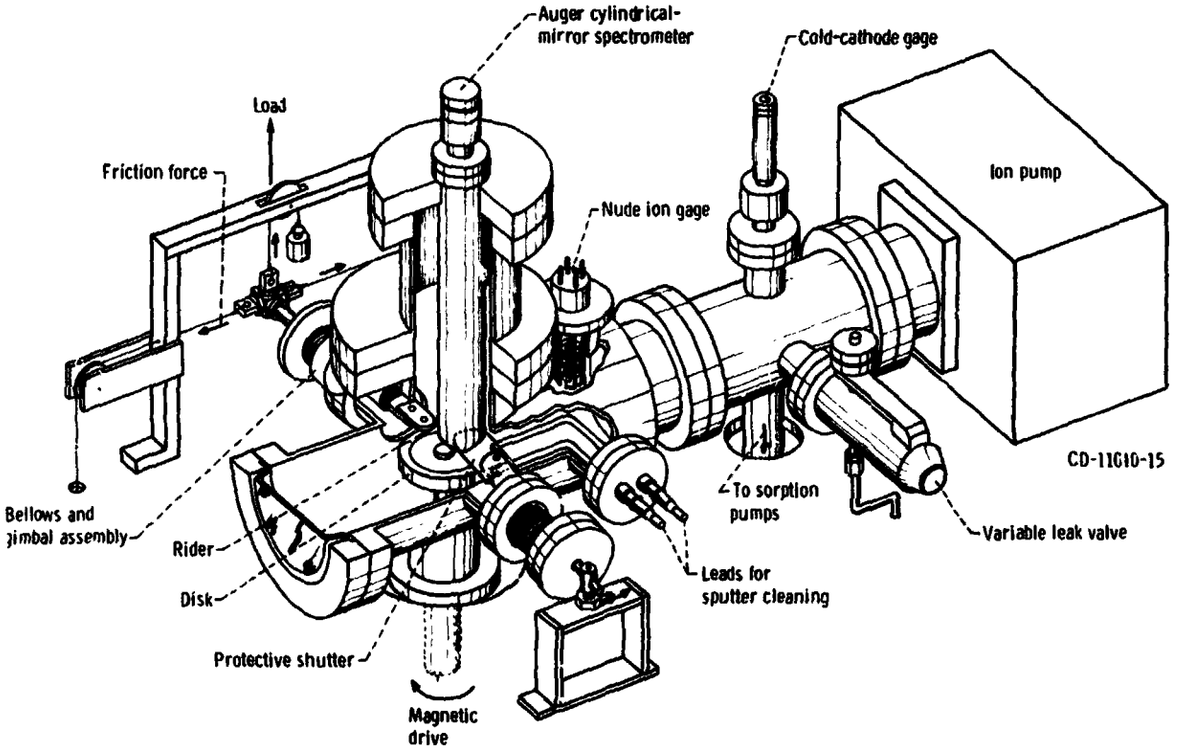

Figure 2. - Friction apparatus with Auger spectrometer.

(a) Tungsten prior to contact. Voltage, 13.0 kilovolts; liquid-nitrogen cooling.

Figure 2. - Field ion micrographs of tungsten-gold contact. Image gas, helium.

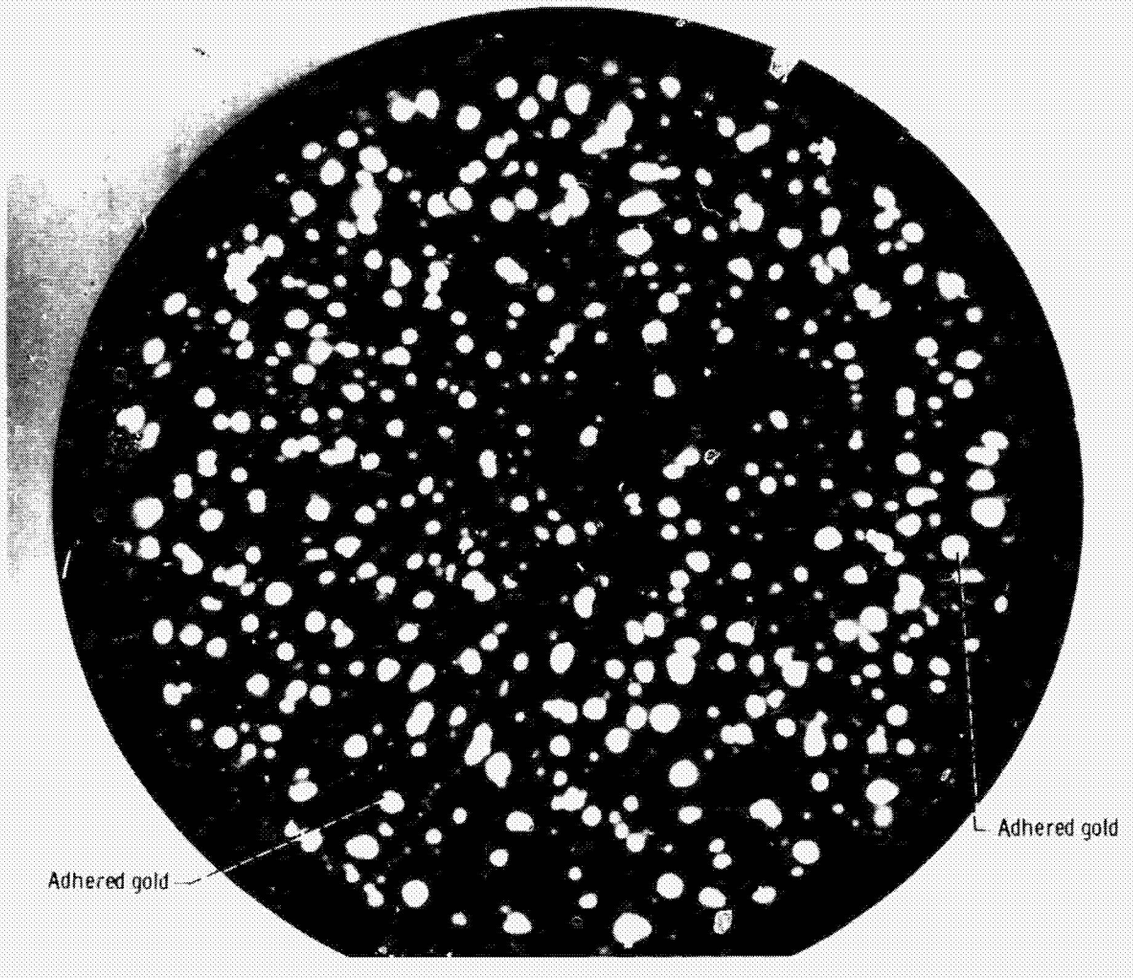

(b) Tungsten after gold contact at 11.0 kilovolts; liquid-nitrogen cooling.

Figure 3. Continued.

(c) Tungsten after gold contact at 13.0 kilovolts with voltage raised to 14.5 kilovolts for 30 seconds; liquid-helium cooling.

Figure 3. Concluded.

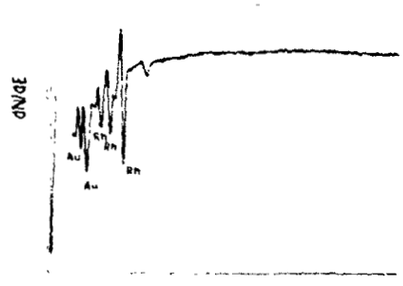

Figure 4. - Auger emission spectrum for a rhodium (111) single crystal surface after a single pass in sliding of a gold (111) crystal across the rhodium surface. Sliding velocity 0.7 mm/min, load 10 grams, 10^{-10} torr and 23° C.

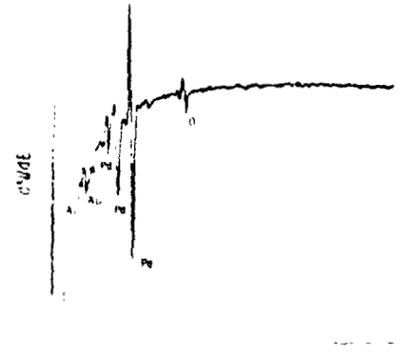

Figure 5. - Auger emission spectrum for a palladium (111) surface containing oxide after a single pass sliding of a gold (111) crystal across the surface. Sliding velocity 0.7 mm/min, load 10 grams, 10^{-10} torr and 23° C.

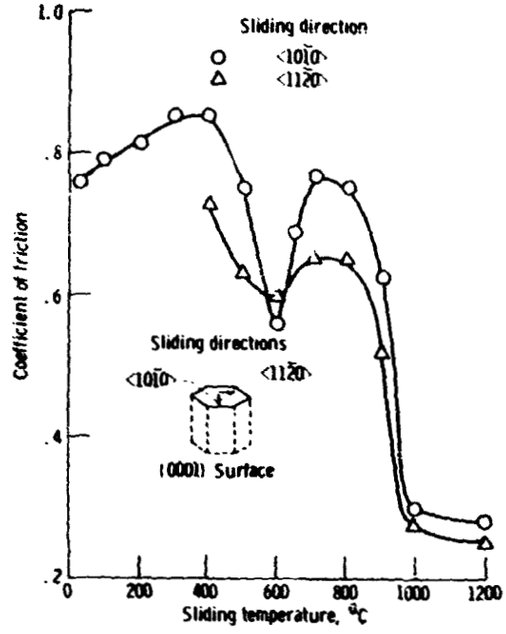

Figure 6. - Effect of temperature on coefficient of friction for silicon carbide (0001) surface sliding against an iron rider. The iron rider was argon ion sputter cleaned before experiments. Normal load, 0.2 N; vacuum, 10 n Pa.

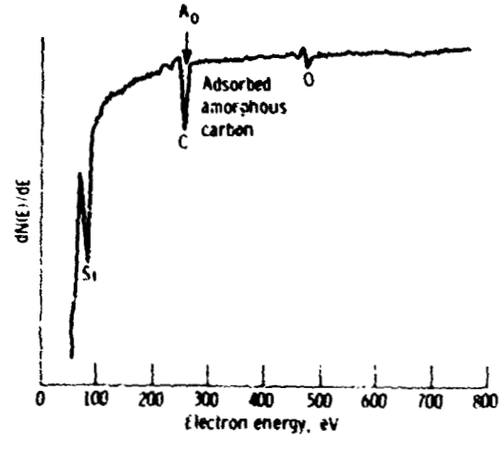

Figure 7. - Auger spectrum of silicon carbide (0001) surface after bake out.

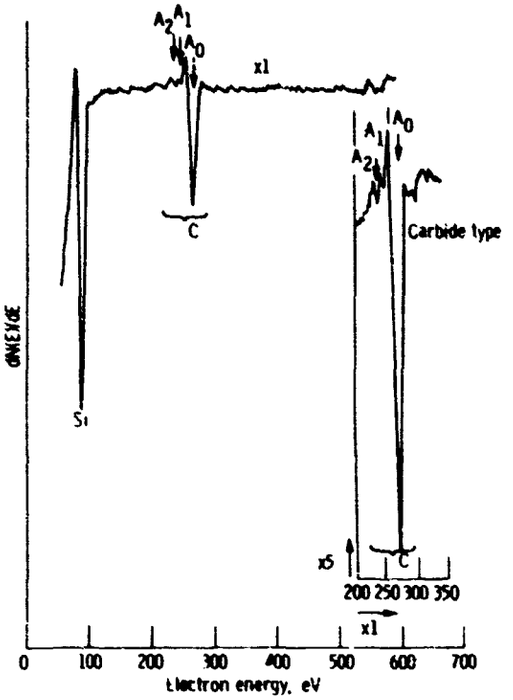

Figure 8. - Auger spectrum of silicon carbide surface after preheating at 800° C for 3 hr in a vacuum of 10 n Pa.

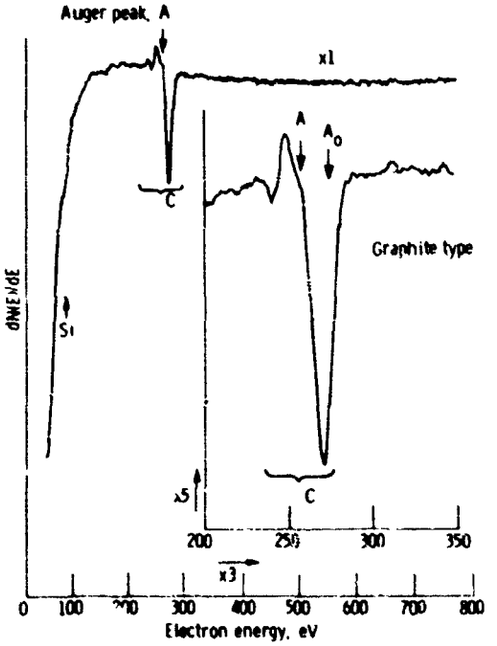

Figure 9. - Auger spectrum of silicon carbide surface after preheating at 1500° C for 3 hr in a vacuum 10 n Pa.

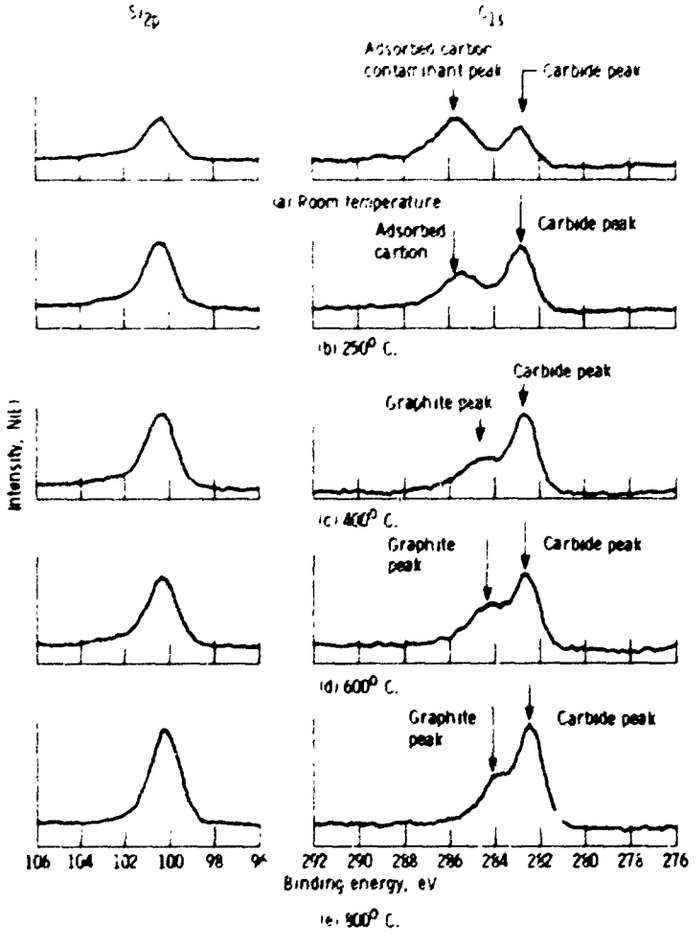

Figure 10. - Representative Si_{2p} and C_{1s} XPS peaks on silicon carbide (0001) surface preheated at various temperatures to 800° C.

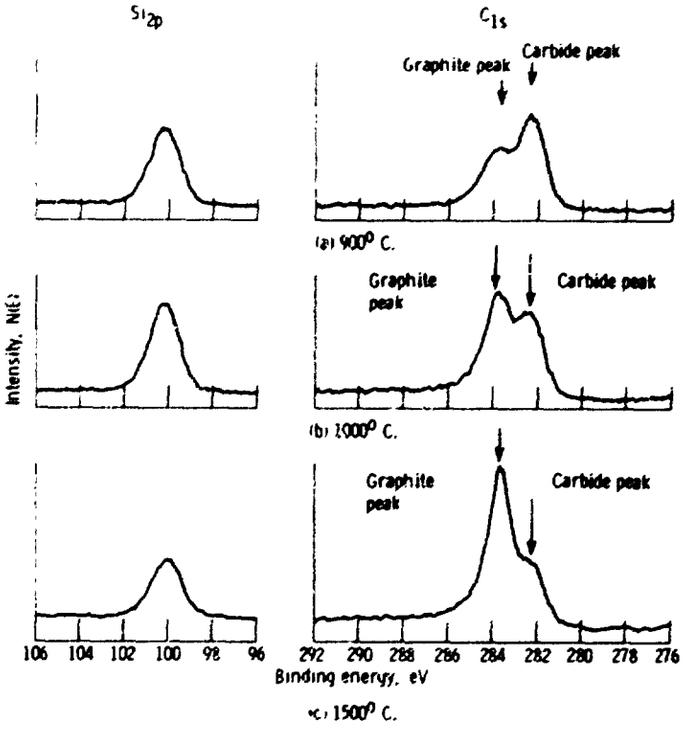

Figure 11. - Representative Si_{2p} and C_{1s} and XPS peaks of the silicon carbide (0001) surface preheated at various temperatures from 900° to 1500° C.

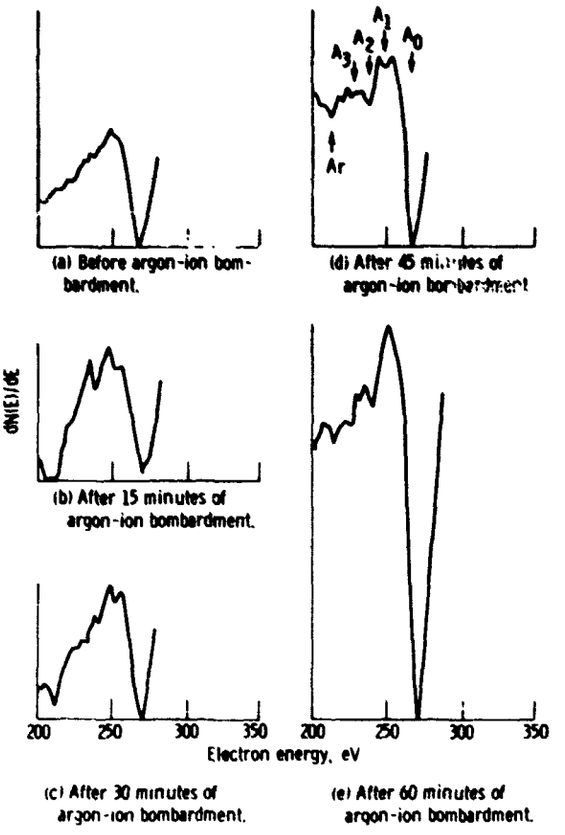

Figure 12. - Comparison of fine structure of the carbon Auger emission spectra for diamond.

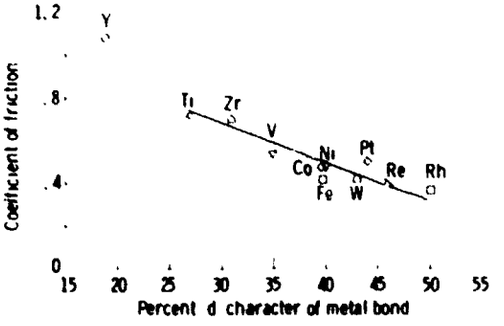

Figure 13. - Coefficient of friction as function of percent of metal d bond character for single-crystal diamond (111) surface in sliding contact with transition metals in vacuum. Sliding direction, $\langle 1\bar{1}0 \rangle$; sliding velocity, 3×10^{-3} m/min; load, 0.05 to 0.3 N; room temperature; vacuum pressure, 10^{-8} Pa.

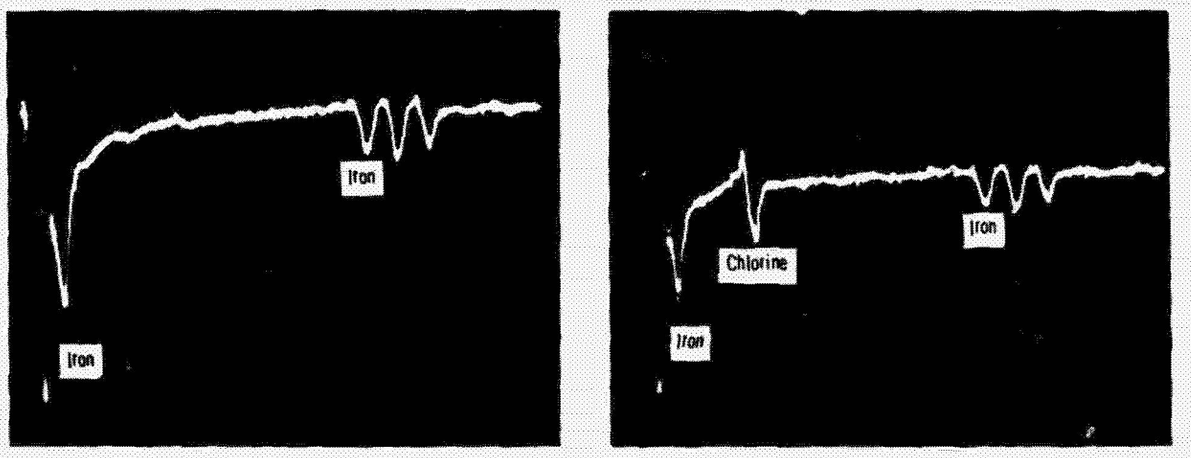

(a) Sputter-cleaned iron.

(b) Iron exposed to 10^{-2} torr-second (10^{4} langmuirs) of benzyl chloride.

Figure 14. - Auger spectra of clean and chloride-covered iron.

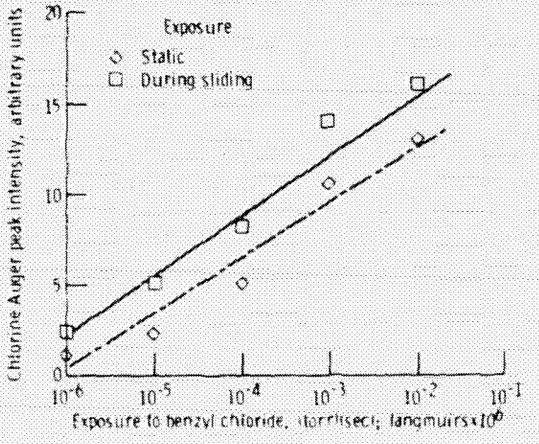

Figure 15. - Chlorine Auger peak intensity as function of iron exposure to benzyl chloride, both static and during sliding. Sliding velocity, 30 centimeters per minute; load, 100 grams; temperature, 23° C.

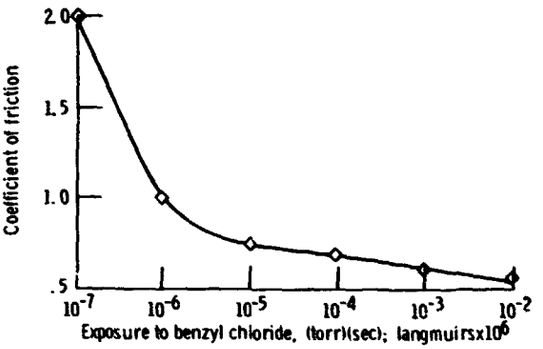

Figure 16. - Coefficient of friction as function of exposure to benzyl chloride for iron-coated aluminum oxide sliding on iron. Sliding velocity, 30 centimeters per minute; load, 100 grams; temperature, 23° C.

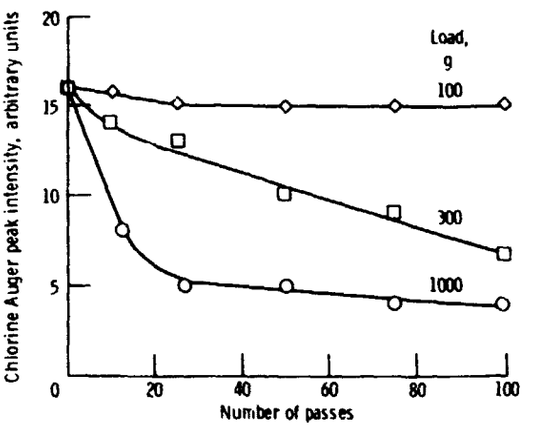

Figure 17. - Change in Auger chlorine peak intensity with number of repeated passes over same iron surface at various loads. Surface exposed to 10^{-2} torr-second (10^4 langmuirs) of benzyl chloride prior to sliding.